Selective Surface Functionalization and Metal Deposition in the Micropores of Mesoporous Silica SBA-15

Chia-Min Yang,*,† Hsing-An Lin,† Bodo Zibrowius,‡ Bernd Spliethoff,‡ Ferdi Schüth,‡ Sz-Chian Liou,§ Ming-Wen Chu,§ and Cheng-Hsuan Chen§

Department of Chemistry, National Tsing Hua University, Hsinchu 30013, Taiwan, Max-Planck-Institut für Kohlenforschung, Kaiser-Wilhelm-Platz 1, D-45470 Mülheim an der Ruhr, Germany, and Center for Condensed Matter Sciences, National Taiwan University, Taipei 10617, Taiwan

Received January 5, 2007. Revised Manuscript Received March 30, 2007

A procedure for the selective surface functionalization of the mesopores and micropores of mesoporous silica SBA-15 has been developed. The resulting bifunctional material has been used to incorporate Pd nanoparticles in the micropores. The method described provides a general route for creating different local environments within the nanometer-sized pore structure and for the selective deposition of guest species in the micropores of this type of bimodal porous materials.

Introduction

Ordered mesoporous materials have attracted wide interest in fields such as catalysis, separation processes, regulated transport, and immobilization of biomolecules.[1−5] Especially interesting for these applications are large-pore mesoporous silica materials prepared using Pluronic-type triblock poly(ethylene oxide)−poly(propylene oxide)−poly(ethylene oxide) ($EO_nPO_mEO_n$) copolymers as structural directing agents (SDAs).[3,6−8] In addition to the primary mesopores, these materials generally have micropores in the pore walls originating from the occlusion of hydrophilic EO chains in silica matrix during the synthesis.[9−12] The contribution of the micropores to the total pore volume can be very high: a microporosity of up to 30% has been reported for SBA-15, a mesoporous silica synthesized using Pluronic P-123 ($EO_{20}PO_{70}EO_{20}$, P123).[10] A bimodal pore structure may bring great opportunities in advanced applications, provided that methods of selective deposition of functional groups or guest species in either one or the other pore system are developed.

With the intention to make use of the unique pore arrangement of SBA-15, we report in this paper a method for the selective functionalization of the surfaces of the two pore types and the subsequent deposition of metal nanoparticles within the micropores. As shown in Scheme 1 and described in detail in the Experimental Section, the mesopores of as-synthesized SBA-15 are first vacated by treatment with sulfuric acid, during which the accessible part of P123 is cleaved and removed.[13−15] The exposed mesopore surface and the external surface of SBA-15 are functionalized with trimethylchlorosilane (TMCS). Subsequently, the material is heated to 250 °C to vacate the micropores of the material while leaving the trimethylsilyl (TMS) groups intact. The open micropores are then functionalized using trivinylchlorosilane (TVCS), and the resulting bifunctional SBA-15 is allowed to react with dichlorobis(acetonitrile)palladium ($PdCl_2(MeCN)_2$) to form metal complexes[16] in the micropores. Subsequent reduction produces a material with fully accessible mesopores and Pd nanoparticles in the micropores. In the present paper, we also report on the catalytic activity of the thus prepared Pd-containing nanocomposites for the Heck reaction.

* Corresponding author. Tel: 886-3-5731282. Fax: 886-3-5165521. E-mail: cmyang@mx.nthu.edu.tw.
† National Tsing Hua University.
‡ Max-Planck-Institut für Kohlenforschung.
§ National Taiwan University.

(1) Sayari, A.; Hamoudi, S. *Chem. Mater.* **2001**, *13*, 3151.
(2) Schüth, F.; Schmidt, W. *Adv. Mater.* **2002**, *14*, 629.
(3) Soler-Illia, G. J. A. A.; Sanchez, C.; Lebeau, B.; Patarin, J. *Chem. Rev.* **2002**, *102*, 4093.
(4) Stein, A. *Adv. Mater.* **2003**, *15*, 763.
(5) Yiu, H. H. P.; Wright, P. A. *J. Mater. Chem.* ***2005***, *15*, 3960.
(6) (a) Zhao, D.; Feng, J.; Huo, Q.; Melosh, N.; Fredrickson, G. H.; Chmelka, B. F.; Stucky, G. D. *Science* **1998**, *279*, 548. (b) Zhao, D.; Huo, Q.; Feng, J.; Chmelka, B. F.; Stucky, G. D. *J. Am. Chem. Soc.* **1998**, *120*, 6024. (c) Choi, M.; Heo, W.; Kleitz, F.; Ryoo, R. *Chem. Commun.* **2003**, 1340.
(7) (a) Kleitz, F.; Liu, D.; Anilkumar, G. M.; Park, I.-S.; Solovyov, L. A.; Shmakov, A. N.; Ryoo, R. *J. Phys. Chem. B.* **2003**, *107*, 14296. (b) Kleitz, F.; Solovyov, L. A.; Anilkumar, G. M.; Choi, S. H.; Ryoo, R. *Chem. Commun.* **2004**, 1536. (c) Kim, T. W.; Ryoo, R.; Kruk, M.; Gierszal, K. P.; Jaroniec, M.; Kamiya, S.; Terasaki, O. *J. Phys. Chem. B.* **2004**, *108*, 11480. (d) Kim, T. W.; Kleitz, F.; Paul, B.; Ryoo, R. *J. Am. Chem. Soc.* **2005**, *127*, 7601.
(8) Stein, A. *Adv. Mater.* **2003**, *15*, 763.
(9) (a) Kruk, M.; Jaroniec, M.; Ko, C. H.; Ryoo, R. *Chem. Mater.* **2000**, *12*, 1961. (b) Ryoo, R.; Ko, C. H.; Kruk, M.; Antochshuk, V.; Jaroniec, M. *J. Phys. Chem. B.* **2000**, *104*, 11465.
(10) Galarneau, A.; Cambon, H.; Di Renzo, F.; Ryoo, R.; Choi, M.; Fajula, F. *New J. Chem.* **2003**, *27*, 73.
(11) Impéror-Clerc, M.; Davidson, P.; Davidson, A. *J. Am. Chem. Soc.* **2000**, *122*, 11925.
(12) Ravikovitch, P. I.; Neimark, A. V. *J. Phys. Chem. B.* **2001**, *105*, 6817.
(13) (a) Yang, C. M.; Zibrowius, B.; Schmidt, W.; Schüth, F. *Chem. Mater.* **2003**, *15*, 3739. (b) Yang, C. M.; Zibrowius, B.; Schmidt, W.; Schüth, F. *Chem. Mater.* **2004**, *16*, 2918.
(14) (a) Yang, C. M.; Zibrowius, B.; Schüth, F. *Chem. Commun.* **2003**, 1772. (b) Yang, C. M.; Wang, Y. Q.; Zibrowius, B.; Schüth, F. *Phys. Chem. Chem. Phys.* **2004**, *6*, 2461.
(15) (a) Wang, Y. Q.; Yang, C. M.; Zibrowius, B.; Spliethoff, B.; Lindén, M.; Schüth, F. *Chem. Mater.* **2003**, *15*, 5029. (b) Wang, Y. Q.; Zibrowius, B.; Yang, C. M.; Spliethoff, B.; Schüth, F. *Chem. Commun.* **2004**, 46.
(16) Dedieu, A. *Chem. Rev.* **2000**, *100*, 543.

10.1021/cm070036r CCC: $37.00
Published on Web 05/25/2007

Scheme 1. Schematic Representation of Selective Surface Functionalization and Selective Deposition of Pd Nanoparticles in the Micropores of SBA-15

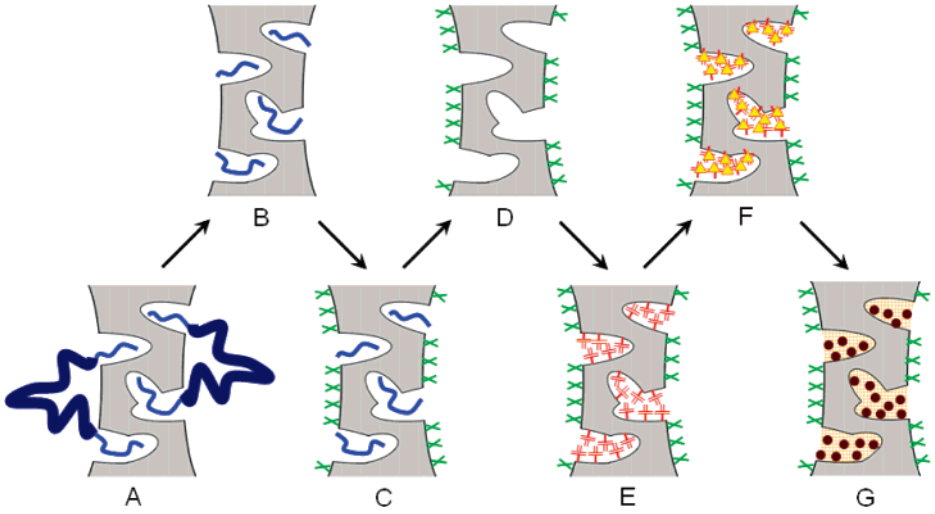

The described method of selective surface functionalization and metal incorporation is versatile and can also be applied to prepare multifunctional materials with other surface functionalities and metals using other bimodal (micro/mesoporous) silica materials. The resulting nanocomposites are distinct from reported materials with nanostructured metals in mesoporous silicas[17] and should have interesting properties for catalysis and other applications. Recently, Yuranov et al. have claimed the selective synthesis of Pd nanoparticles in the micropores of SBA-15 from which the template was removed by ethanol extraction.[18] However, ethanol extraction cannot remove the template completely[9a] and the synthesis route described might not be applicable for other metals.

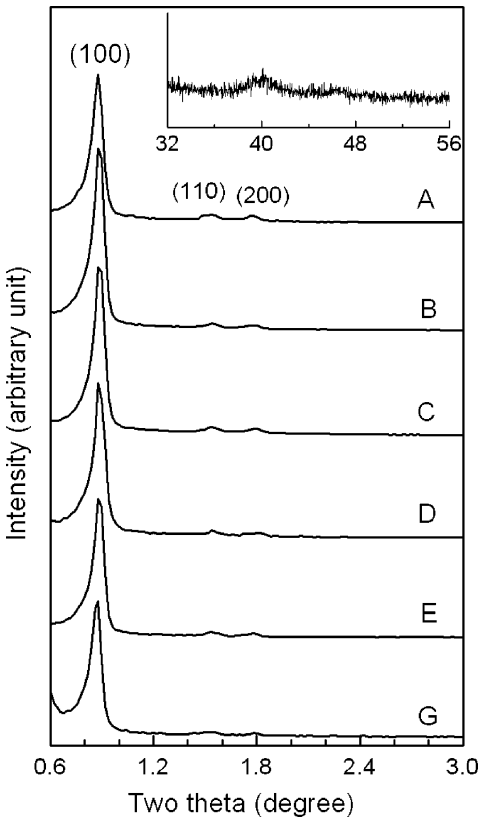

Figure 1. PXRD patterns of selected samples. Inset: wide-angle PXRD of sample G.

Experimental Section

Synthesis. The synthesis of mesoporous silica SBA-15 was performed under low (0.3 M) acidity conditions according to a previously reported procedure.[6c] A typical synthesis started from the preparation of a hydrochloric acid (HCl) solution of P123. Tetraethoxysilane (TEOS) was then added to the copolymer solution and the mixture was stirred at 35 °C for 20 h. The molar composition was TEOS:HCl:H_2O:P123 1:0.54:100:0.017. After aging at 50 °C for 1 day, the product was filtered and dried at 90 °C. The resulting as-synthesized SBA-15 is referred to as sample A. For the removal of the template,[13] 1.0 g of sample A was stirred in 100 mL of 45 wt % H_2SO_4 solution at 95 °C for 24 h. The product (sample B) was washed and dried at 90 °C. The first functionalization was accomplished by pouring sample B into the toluene solution of TMCS. After stirring for 1 h, the material was filtered, washed, and dried (sample C). To vacate the micropores, sample C was heated in air at a heating rate of 1 °C min^{-1} to 250 °C and was kept at this temperature for 3 h. The resulting sample D was further reacted with TVCS in toluene for 3 h. The product (sample E) was then recovered after subsequent washing and drying steps.

To incorporate the metal, an excess amount of dichloromethane solution of $PdCl_2(MeCN)_2$ was added to sample E. The powder took up the color of the metal salt, and the resulting material (sample F) was filtered, washed with dichloromethane, and dried under ambient conditions. The metal reduction to obtain sample G was conducted by heating sample F in hydrogen flow at a heating rate of 1 °C/min to 300 °C and keeping it at this temperature for 3 h.

The selective surface functionalization was also performed on mesoporous silica SBA-15 synthesized under high (1.6 M) acidity conditions. The synthesis of this silica material was the same as that for SBA-15 synthesized under low acidity conditions, except for the aging temperature of 90 °C and the molar composition of

(17) (a) Taguchi, A.; Schüth, F. *Microporous Mesoporous Mater.* **2005**, *77*, 1. (b) Yang, H.; Zhao, D. *J. Mater. Chem.* **2005**, *15*, 1217. (c) Descalzo, A. B.; Martínez-Máñez, R.; Sancenón, F.; Hoffmann, K.; Rurack, K. *Angew. Chem., Int. Ed.* **2006**, *45*, 5924. (d) Fukuoka, A.; Ichikawa, M. *Top. Catal.* **2006**, *40*, 103.
(18) Yuranov, I.; Kiwi-Minsker, L.; Buffat, Ph.; Renken, A. *Chem. Mater.* **2004**, *16*, 760.

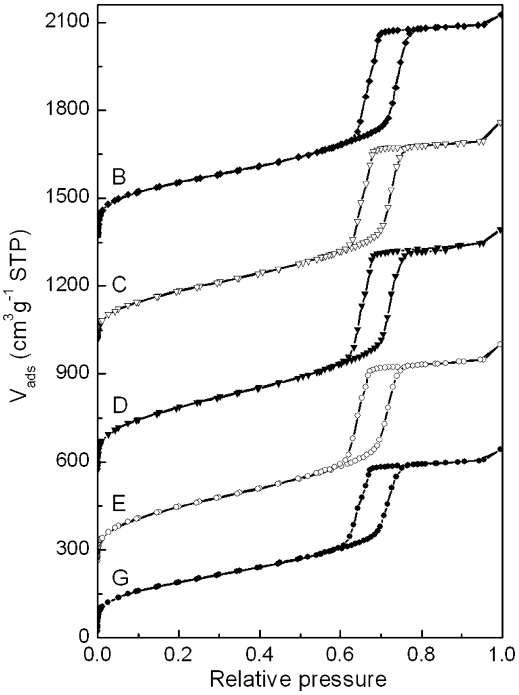

Figure 2. Nitrogen physisorption isotherms of selected samples. The isotherms are shifted by 250, 550, 1000, and 1350 cm^3 g^{-1} STP, respectively.

TEOS:HCl:H_2O:P123 1:5.9:193:0.017. The as-synthesized SBA-15 is denoted as sample A′. After the same treatment with sulfuric acid as described above, the product (sample B′) was functionalized with dimethyldichlorosilane (DMDS) instead of TMCS by following the same reaction protocol, resulting in sample C′. After vacating the micropores by heating at 250 °C, the material (sample D′) was further functionalized with TVCS to produce sample E′. By following the same protocol of metal incorporation and reduction, samples F′ and G′ were prepared.

The method of selective surface functionalization and metal deposition is highly reproducible. The synthesis was repeated several times with essentially identical results.

Characterizations. Powder X-ray diffraction (PXRD) data were obtained on a Mac Science 18MPX diffractometer using Cu Kα radiation. Nitrogen physisorption isotherms were measured at 77 K using a Quantachrome Autosorb-1-MP instrument. The pore diameters and the pore size distributions were calculated from the desorption branch using the Barrett−Joyner−Halenda (BJH) method. The BET surface areas were calculated from the adsorption branches in the relative pressure range of 0.05−0.20, and the total pore volumes were evaluated at a relative pressure of 0.95. For *t*-plot analyses, the Harkins−Jura equation with standard parameters obtained from nonporous reference material was used. The solid-state NMR spectra were measured on a Bruker DSX400WB spectrometer or a Bruker Avance 500WB spectrometer using 4 mm MAS probes at a spinning rate of 6.5 kHz or 10 kHz, respectively.[13,19] CO static chemisorption was performed using a Quantachrome Autosorb-1C at 40 °C. Prior to the measurements, the samples were activated at 200 °C for 12 h in helium. The dispersions and sizes of Pd particles in the samples were estimated using a shape factor of 6 and a Pd:CO stoichiometry of 1:1. The transmission electron microscope (TEM) images were obtained with a Hitachi HF2000 electron microscope. For the scanning transmission electron microscopy (STEM) and energy-dispersive X-ray spectroscopy (EDX) investigations, which were performed on a FEI field-emission microscope (Tecnai G^2 F20, operated at 200 kV), the sample was embedded in a resin and ultramicrotomed into slices with a thickness of about 50 nm. The inductively coupled plasma atomic emission spectroscopy (ICP-AES) data were obtained using a Jarrell-Ash-ICAP 9000 device.

Table 1. Structural Properties of Samples A−E and G[a]

sample	a_0/nm	d^b/nm	w/nm	S_{BET}/ m^2 g^{-1}	$V_t{}^c$/ cm^3 g^{-1}	$V_m{}^d$/ cm^3 g^{-1}
A	10.5	NA[e]	NA	NA	NA	NA
B	10.5	6.5	4.0	609	0.90	0.03
C	10.5	6.3	4.2	564	0.88	0.01
D	10.5	6.3	4.2	618	1.01	0.24
E	10.5	6.3	4.2	601	0.86	0.11
G	10.5	6.3	4.2	547	0.72	0.04

[a] a_0, unit cell parameter; d, mesopore diameter; w, pore wall thickness; S_{BET}, BET surface area; V_t, total pore volume; V_m, micropore volume. [b] Calculated from the desorption branch using the BJH method. [c] Calculated at $P/P_0 = 0.95$. [d] Calculated from the *t*-plot analysis. [e] NA, not available.

Results and Discussion

The as-synthesized SBA-15 (sample A) had an ordered hexagonal structure, as indicated by the intense (100), (110), and (200) reflections in the small-angle region of its powder X-ray diffraction (PXRD) pattern shown in Figure 1. The cell parameter (a_0) of sample A was 10.5 nm, and this remained unchanged after the material was subjected to further steps of the preparative procedures. Sample A was first treated with sulfuric acid to vacate the mesopores. The nitrogen physisorption isotherm of the resulting sample B, as shown in Figure 2, exhibits a sharp step with a H1-type hysteresis loop corresponding to the filling of uniform mesopores with open cylindrical geometry.[20] The calculated mesopore diameter for sample B is 6.5 nm. Other structural properties of the samples derived from PXRD and nitrogen sorption measurements are summarized in Table 1.

The changes caused by each step of the preparative procedure were monitored by ^{13}C CP/MAS and ^{29}Si MAS NMR spectroscopy (cf. Figure 3). The ^{13}C NMR spectrum of sample B indicates that the PO blocks of P123 were removed preferentially from the as-synthesized SBA-15, and the line at 70.4 ppm characteristic of remaining EO groups is clearly visible.[13] This is in accordance with the *t*-plot analysis of the sorption isotherm of sample B, which suggests that the material had a very small micropore volume of 0.03 cm^3 g^{-1}. The TMS groups were then grafted onto the mesopore surface and the external surface by reaction with TMCS, resulting in sample C. The presence of grafted species is evident from the additional line of the methyl groups at −0.9 ppm in the ^{13}C NMR spectrum and the resonance of TMS groups at about 14 ppm in the ^{29}Si NMR spectrum. The grafting also reduced the relative intensities of the Q^3 and Q^2 lines (Q^n: $Si(OSi)_n(OH)_{4-n}$): Q^2:Q^3:Q^4 = 3:37:60 and 2:29:69 for samples B and C, respectively. The TMS/Q intensity ratio of sample C is about 9.9:100, suggesting that around a quarter of all silanol groups present in sample B had reacted with TMCS. The presence of TMS

(19) Yang, C. M.; Liu, P. H.; Ho, Y. F.; Chiu, C. Y.; Chao, K. J. *Chem. Mater.* **2003**, *15*, 275.

(20) Sing, K. S. W.; Everett, D. H.; Haul, R. A. W.; Moscou, L.; Pierotti, R. A.; Rouquerol, J.; Siemieniewska, T. *Pure Appl. Chem.* **1985**, *57*, 603.

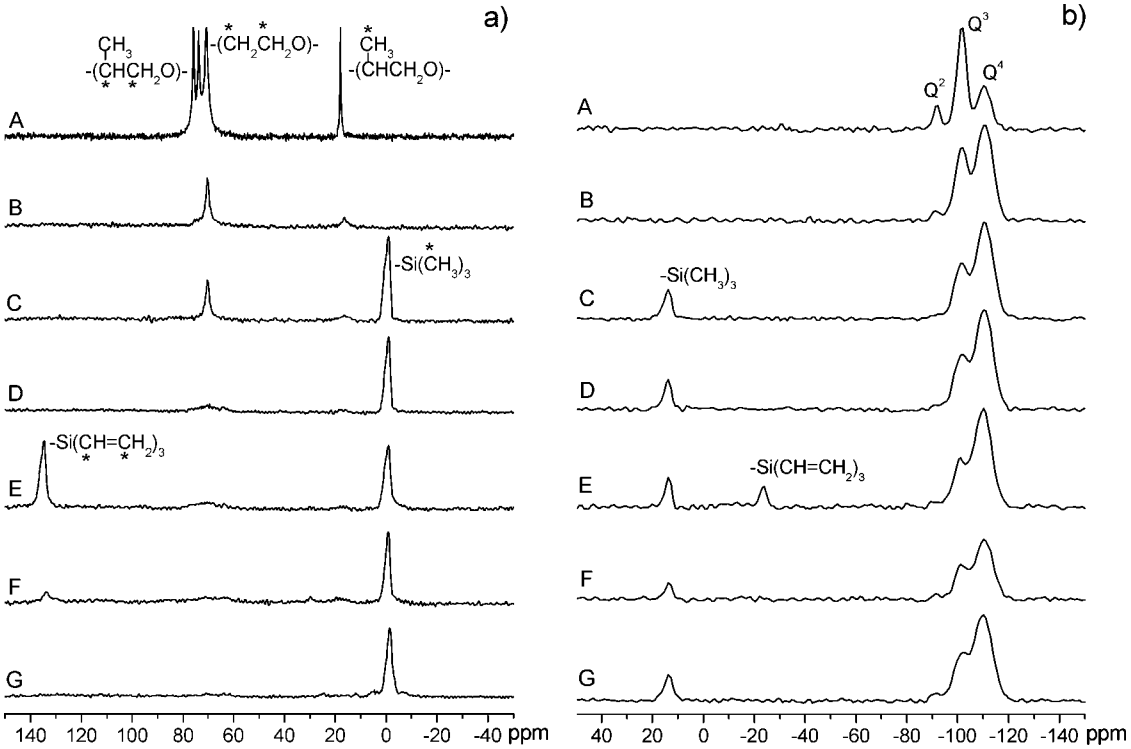

Figure 3. ^{13}C CP/MAS (a) and ^{29}Si MAS (b) NMR spectra of samples A−G.

groups in sample C had limited influence on the nitrogen sorption, and the analysis of its isotherm gave a slightly smaller mesopore diameter of 6.3 nm and again a very small micropore volume of 0.01 $cm^3\ g^{-1}$.

Consistent with the thermal decomposition of the EO chains, the line attributed to EO groups is missing in the ^{13}C NMR spectrum of sample D. On the other hand, the thermal treatment nearly had nearly no influence on the ^{29}Si NMR spectrum of the material, indicating that most of the TMS groups were not affected by the thermal treatment. The sorption analysis suggested that sample D had the same mesopore diameter of 6.3 nm but a rather large micropore volume of 0.24 $cm^3\ g^{-1}$. Hence, the micropores can be assumed to be fully accessible and not blocked by the TMS groups on the surface of the mesopores.

The second functionality was introduced into the material by reacting sample D with TVCS. The ^{13}C NMR spectrum of the resulting sample E exhibits an additional line at 135 ppm that can be assigned to the vinyl carbons of the grafted TVS groups.[21] The silicon atoms of the TVS groups give rise to an additional line at −24 ppm in the ^{29}Si NMR spectrum of sample E. The intensity ratio of TVS, TMS, and Q lines in this spectrum is about 5.8:10.5:100. Since the reactive silanol groups in the mesopores and on the outer surface of sample D had already been passivated by TMS groups, TVCS should preferentially react with silanol groups in the micropores. The anchored TVS groups lowered the micropore volume to 0.11 $cm^3\ g^{-1}$ without reducing the mesopore diameter. However, the physicochemical parameters derived from sorption isotherms should not be taken as precise data but should only be used for comparison. The different surface properties of the mesopores and micropores of the various samples may affect the sorption behavior of the materials to a certain extent.

Upon mixing sample E with $PdCl_2(MeCN)_2$, the vinyl groups are thought to displace the weakly coordinated MeCN ligands on the palladium to form π-bonded complexes.[22] The introduction of palladium had striking effects on the NMR spectra of sample F (cf. Figure 3). In both spectra, the intensities of the lines of the TVS groups are drastically reduced. Furthermore, the overall intensity of the ^{29}Si NMR spectrum is significantly lower than for all other spectra recorded under identical conditions. Since Pd−vinyl π-complexes may react further via carbocation intermediates,[22] a plausible explanation is that some paramagnetic species are formed. After reduction of the metal by hydrogen at 300 °C, the lines stemming from the TVS groups completely disappeared in both the ^{29}Si and the ^{13}C NMR spectra of the resulting sample G. The wide-angle PXRD pattern of sample G (the inset in Figure 1) shows very broad and weak reflections attributed to metallic Pd. In addition, analyses of its sorption isotherm indicated that the micropore volume of sample G was reduced to 0.04 $cm^3\ g^{-1}$ while no blocking of the mesopores was observed. These results strongly suggest that the reduced Pd formed very small nanoparticles located inside the micropores of SBA-15.

The Pd nanoparticles in sample G exhibit good stability against possible sintering to form larger particles in the mesopores or on the outer surface of SBA-15. Figure 4 shows the so-called Z-contrast STEM images of the sample after further heating to 550 °C in hydrogen flow (sample H). From the characteristic dark contrast observed in the image along

(21) (a) Levy, G. C.; White, D. M.; Cargioli, J. D. *J. Magn. Reson.* **1972**, *8*, 280. (b) Zhun', V. I.; Zhun', A. B.; Bereza, E. Yu.; Chernyshev, E. A. *Russ. J. Gen. Chem.* **2000**, *70*, 1746.

(22) (a) Sen, A.; Lai, T. W. *J. Am. Chem. Soc.* **1981**, *103*, 4627. (b) Sen, A. *Acc. Chem. Res.* **1988**, *21*, 421. (c) Hahn, C.; Morvillo, P.; Vitagliano, A. *Eur. J. Inorg. Chem.* **2001**, 419.

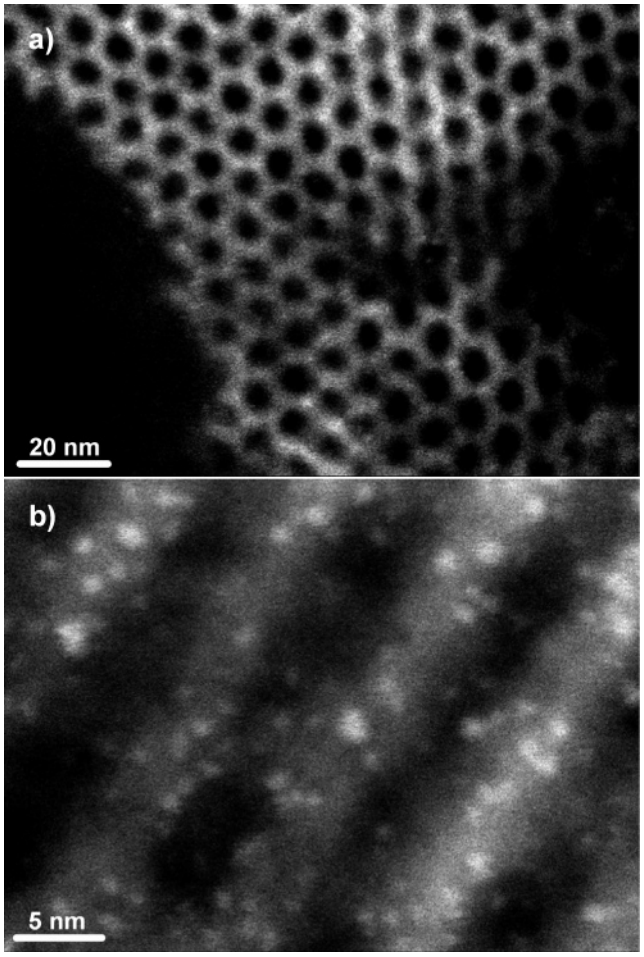

Figure 4. STEM images of sample H viewed along (a) and perpendicular to (b) the axis of the hexagonally arranged mesopores.

the axis of the hexagonally arranged mesopores (Figure 4a), it is obvious that the mesopores are empty, free from any Pd nanoparticles. The rather inhomogeneous bright contrast observed for the walls of the mesopores (Figure 4a) could then be related to the Pd nanoparticles, considering that Pd is appreciably heavier than the other constituent elements. Figure 4b shows an image of the sample observed along the direction perpendicular to the pore axis. It reveals a considerable amount of bright spots, resulting from the Pd nanoparticles, with a size of about 2 nm embedded in the relatively gray contrasts arising from the mesopore walls. As the sample retained such a high dispersion after heating at 550 °C (sample H), a similar dispersion can certainly be assumed for the parent sample G. The energy-dispersive X-ray spectroscopy (EDX) analysis indicated an average Pd loading of about 8.5 wt %, which is consistent with the value of 9.2 wt % from the bulk elemental analysis by inductively coupled plasma atomic emission spectroscopy (ICP-AES). Combining these data with the information on the amount of TVS groups in sample E from ^{29}Si NMR analysis, the estimated molar ratio of loaded Pd to the vinyl groups is around 1:4. This ratio is smaller than what one would expect from the stoichiometry of the ligand-exchange reaction between $PdCl_2(MeCN)_2$ and the vinyl groups.[22] The finding may be attributed to the limited accessibility of TVS groups grafted deeply inside the micropores of SBA-15.

The selective surface functionalization and metal incorporation was also performed on the SBA-15 synthesized under high (1.6 M) acidity conditions with an aging temperature of 90 °C. The cell parameter a_0 of sample A′ was 11.8 nm and remained unchanged during the whole preparative procedure. In this series of samples, DMDS instead of TMCS was used to functionalize the mesopore surface. Figure 5 shows the ^{13}C CP/MAS and ^{29}Si MAS NMR spectra of samples B′−G′. In addition to lines assigned above, the D^n (D^n: $Si(OSi)_n(OH)_{2-n}C_2$) lines stemming from the silicon atoms of dimethylsilyl (DMS) groups are marked. Similar to the data for the previous series of samples (samples B−G), the spectra indicate the selective removal of PO blocks, the functionalization of mesopore surface and external

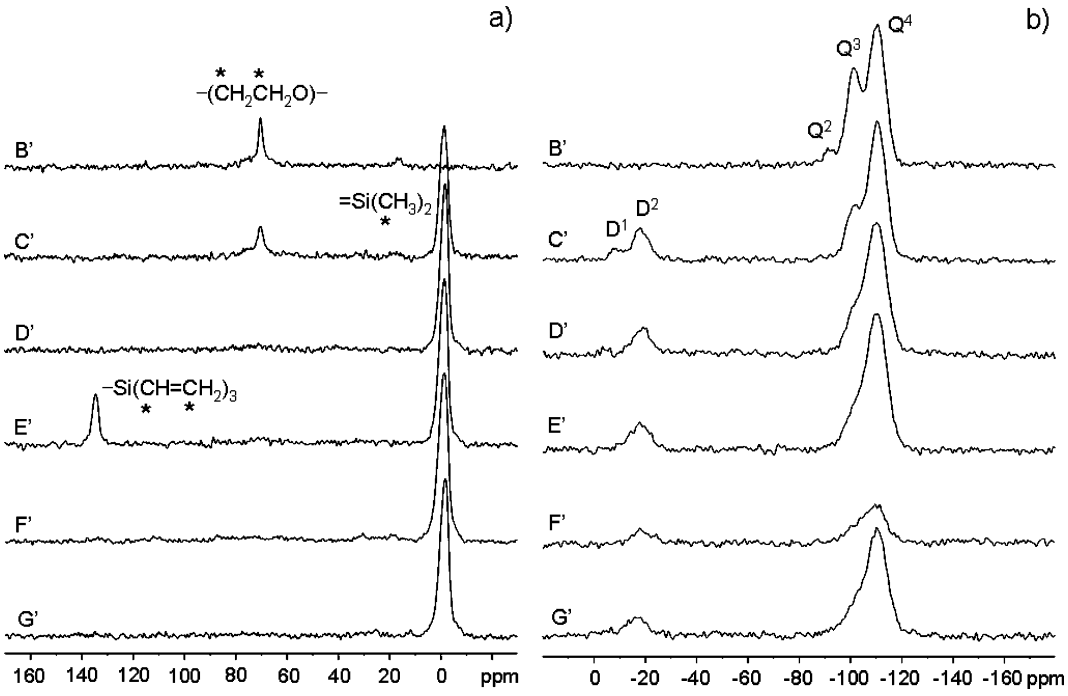

Figure 5. ^{13}C CP/MAS (a) and ^{29}Si MAS (b) NMR spectra of samples B′−G′.

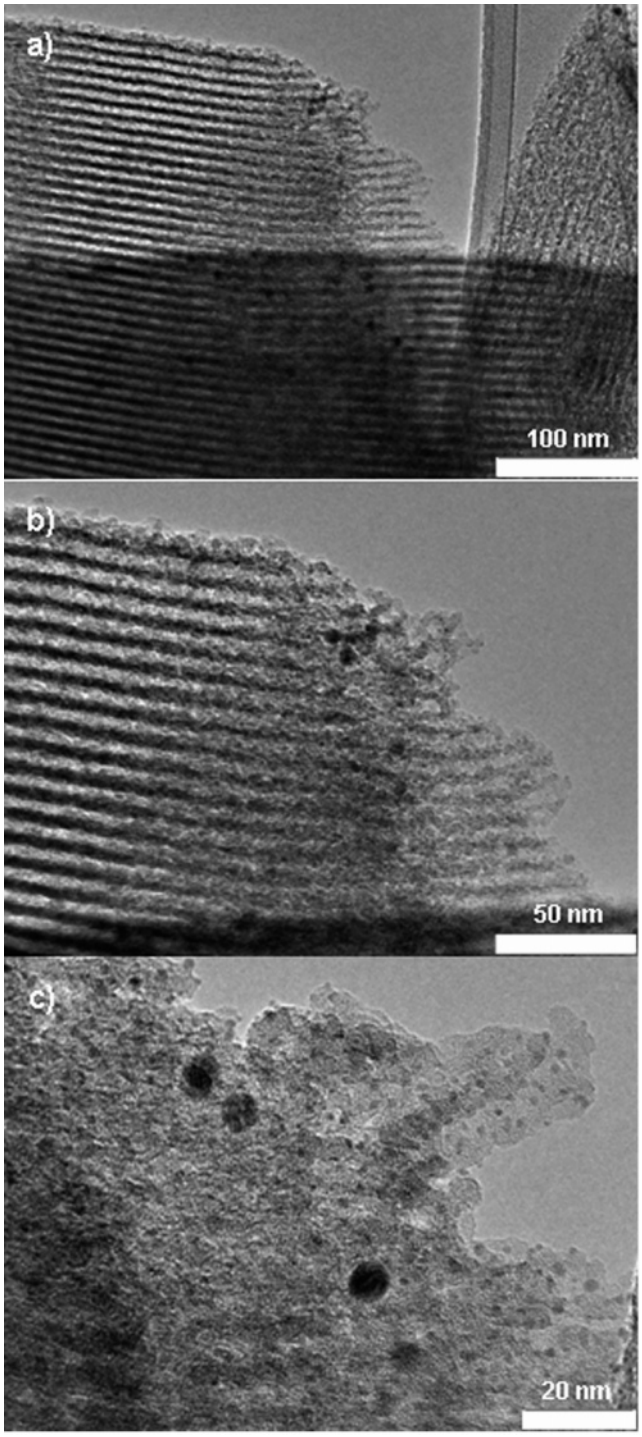

Figure 6. TEM images of sample H′ before (a) and after further exposure to a strong electron beam for 2 min (b) and 5 min (c).

surface with DMS groups, the vacation of micropores by low-temperature calcination, the second functionalization of the open micropores with TVS groups, and the effects of metal incorporation. The physicochemical properties of these samples estimated from the analyses of their nitrogen physisorption isotherms are summarized in Table 2. All the samples have the same mesopore diameter of 8.1 nm, while their micropore volumes and other properties change similarly to those of samples A−G.

The Pd nanoparticles in sample G′ do not sinter upon treatment at 550 °C in hydrogen flow. In the TEM image of sample H′ (Figure 6a), no Pd particles can be seen in the

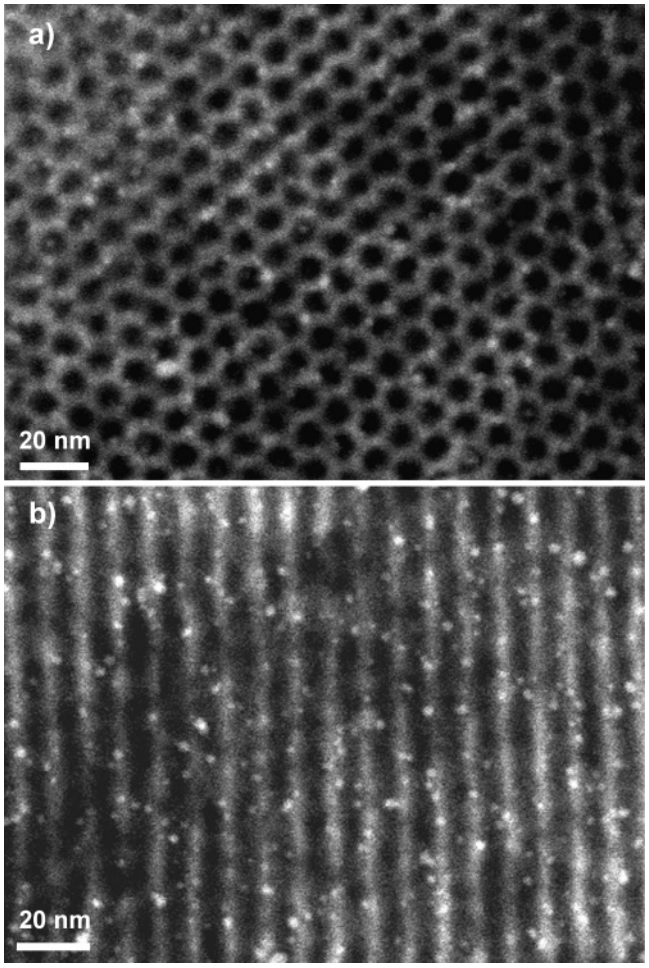

Figure 7. STEM images of sample I viewed along (a) and perpendicular to (b) the axis of the hexagonally arranged mesopores.

Table 2. Structural Properties of Samples A′−E′ and G′ [a]

sample	a_0/nm	d^b/nm	w/nm	S_{BET}/ $m^2\ g^{-1}$	$V_t{}^c$/ $cm^3\ g^{-1}$	$V_m{}^d$/ $cm^3\ g^{-1}$
A′	11.8	NA[e]	NA	NA	NA	NA
B′	11.8	8.1	3.7	615	1.02	0.02
C′	11.8	8.1	3.7	592	0.94	0.02
D′	11.8	8.1	3.7	615	1.04	0.20
E′	11.8	8.1	3.7	615	0.92	0.11
G′	11.8	8.1	3.7	570	0.87	0.03

[a] a_0, unit cell parameter; d, mesopore diameter; w, pore wall thickness; S_{BET}, BET surface area; V_t, total pore volume; V_m, micropore volume. [b] Calculated from the desorption branch using the BJH method. [c] Calculated at $P/P_0 = 0.95$. [d] Calculated from the t-plot analysis. [e] NA, not available.

channel-like mesopores, but there are some darker spots in the silica walls. However, it is difficult to verify from the two-dimensional projection image of a three-dimensional object whether these spots are Pd nanoparticles in the micropores or not. One way to support this interpretation is to expose the sample to a strong electron beam in the microscope for a time sufficient to destroy the ordered mesoscopic structure of the silica host. The embedded Pd clusters would then be released from the micropores and form larger nanoparticles that can be observed by TEM. Parts b and c of Figure 6 show TEM images of the same region as Figure 6a but after further exposure to a strong electron beam for 2 and 5 min, respectively. Comparison of these figures shows that while the contrast for the ordered pore structure

becomes diminished as a result of beam damage, highly dispersed nanoparticles emerge. A few larger Pd particles are also formed in the strong electron beam. The small Pd nanoparticles are very uniform in size, with diameters of 2.0 ± 0.5 nm. This observation supports that the reduced Pd clusters are located preferentially in the micropores of sample H′, for which EDX analysis revealed an average Pd loading of 6.3 wt %.

The unusual stability of the Pd nanoparticles during thermal reduction might be due in part to the interaction between Pd and residual hydrocarbon species in the confined space of the micropores. Further studies by CO chemisorption were carried out to study the chemical environment of the Pd nanoparticles. Surprisingly, both samples G and H exhibited low CO chemisorption capacities and apparently low metal dispersions (20% for sample G and 17% for sample H). The thus estimated Pd particle sizes were 5.6 and 6.5 nm for samples G and H, respectively. The finding seemed contradictory to the results of other investigations, and we reasoned that the low CO chemisorption capacity might be due to a reduced accessibility of the Pd nanoparticles caused by some carbonaceous residues formed from the TVS groups during metal reduction. To substantiate this assumption, sample G was heated in an air flow at 400 °C for 3 h and was then reduced again in a hydrogen flow at 300 °C for 3 h. Indeed, the resulting sample I showed a much higher CO chemisorption capacity than sample G, giving a calculated metal dispersion of 60% and an estimated Pd particle size of 1.9 nm. The Z-contrast STEM images of sample I (Figure 7) also show that the mesopores of SBA-15 are empty and Pd nanoparticles are embedded in the silica walls. It suggests that the Pd nanoparticles in the micropores of SBA-15 can survive the oxidation−reduction treatment to remove the residual hydrocarbon species in the micropores.

Furthermore, the catalytic activities of samples G and I for the Heck reaction with bromobenzene and styrene were tested and compared. The reactions were conducted at 120 °C for 48 h with 0.01 mol % catalyst, *N*,*N*-dimethylacetamide as solvent, and sodium acetate as base but without any phosphine or nitrogen-donor ligands. It was found that while sample I resulted in a reasonable yield of 22%; sample G gave a low yield of 6% under the same reaction conditions. Hence, the results of CO chemisorption and catalytic testing seem to support the idea of restrictions in the accessibility of the Pd nanoparticles in the micropores of sample G that could be eliminated by further treatment.

Conclusions

We have developed a procedure for the selective functionalization of SBA-15 that results in different chemical functionalities on the surfaces of mesopores and micropores. We have also shown that a preferential deposition of Pd precursors in the vinyl-functionalized micropores can be accomplished. The method described in this study provides a general route for creating a heterogeneous local environment within the nanometer-sized pore structure and is highly promising for the preparation of novel nanocomposite materials for catalysis and other applications.

Acknowledgment. The authors thank Mr. Ping-Hsun Lu and Prof. Chun-Chen Liao for help with the catalytic testing. National Science Council of the Republic of China is gratefully acknowledged for financial support under the contract no. NSC 95-2113-M-007-032-MY.

CM070036R